

Electron-nuclear wave-packet dynamics through a conical intersection

 Kilian Hader,¹ Julian Albert,¹ E. K. U. Gross,² and Volker Engel¹
¹*Institut für Physikalische und Theoretische Chemie, Universität Würzburg, Emil-Fischer-Strasse 42, Campus Nord, 97074 Würzburg, Germany*
²*Max-Planck Institut für Mikrostrukturphysik, Weinberg 2, D-06120 Halle, Germany*

(Received 29 November 2016; accepted 26 January 2017; published online 17 February 2017)

We investigate the coupled electron-nuclear dynamics in a model system showing a conical intersection (CoIn) between two excited state potential energy surfaces. Within the model, a single electron and nucleus move in two dimensions in an external static field. It is demonstrated that the nuclear density conserves its initial Gaussian shape when directly passing the CoIn, whereas the electronic density remains approximately constant. This is in sharp contrast to the picture which evolves from an analysis within the basis of adiabatic electronic states. There, dramatic changes are seen in the dynamics of the different nuclear components of the total wave function. It is thus documented that, in the case of a highly efficient population transfer between the respective adiabatic states, neither the nuclear nor the electronic density is influenced by the existence of a CoIn. This is the case because the nuclear-electronic wave packet moves on the complete potential energy surface which changes its topology smoothly as a function of all particle coordinates. *Published by AIP Publishing.* [<http://dx.doi.org/10.1063/1.4975811>]

The complete quantum mechanical treatment of molecules is traditionally performed in two steps. First, the electronic Schrödinger equation is solved for a set of fixed nuclear geometries. These electronic structure calculations^{1,2} yield potential energy surfaces $V_m(\mathbf{R})$ depending on the nuclear coordinates \mathbf{R} and on the electronic quantum number m . Within the Born-Oppenheimer approximation,³ the quantum dynamics in a single electronic state is treated.^{4,5} This involves the solution of the Schrödinger equation for the nuclei including only one potential $V_m(\mathbf{R})$. In electronically excited states of molecules, this approximation usually breaks down because strong non-adiabatic couplings between different electronic states are present. Such couplings are often manifested by the so-called *conical intersections* (CoIns)^{6–11} which determine the outcome of many photochemical reactions. The scenario is such that, after the preparation of a nuclear wave packet in an excited state, an ultrafast passage of the CoIn between two excited states takes place. As a consequence, this non-adiabatic transition results in products formed predominantly in the initially un-populated state.

The theoretical description of the quantum dynamics involving conical intersections usually treats nuclear wave packets on coupled diabatic surfaces,¹² and many studies can be found in the literature, see the compilations Refs. 7 and 8. Modern experiments aim at the characterization of signatures of dynamics close to CoIns. Here, for example, pump-probe measurements,^{13–15} femtosecond two-dimensional optical¹⁶ (a theoretical description of such a scheme can be found in Ref. 17), or high harmonic spectroscopy¹⁸ were employed. Also, the use of attosecond X-ray Raman measurements has been proposed.^{19,20}

In the present paper we pose the question of how electrons and nuclei behave during their coupled motion at a conical intersection. This follows our recent work which investigated the dynamics at avoided crossings.²¹ In order to get insight

into this problem, it is necessary to treat the dynamics of electrons and nuclei on the same footing which, for many-particle systems, is simply not possible. Therefore, we concentrate on a model system first introduced by Shin and Metiu^{22,23} for a one-dimensional motion, for later applications see, e.g., Refs. 24–29. The here used extension of the model consists of one electron and one proton moving in two dimensions in an additional static field provided by two fixed ions.³⁰ The particle configuration is displayed in the upper part of Fig. 1. The system exhibits a CoIn at the symmetric configuration with D_{3h} -symmetry. We integrate the time-dependent Schrödinger equation for the coupled motion and monitor the dynamics at times when the electronic-nuclear wave packet passes the conical intersection. This situation is compared to the case where the dynamics, within the adiabatic picture, takes place exclusively in the lower excited state.

Denoting the nuclear and electron coordinates as $\mathbf{R} = (R_x, R_y)$ and $\mathbf{r} = (x, y)$, respectively, the Hamiltonian is (atomic units are employed)

$$H = \frac{\mathbf{p}^2}{2} + \frac{\mathbf{P}^2}{2M} + V(\mathbf{r}, \mathbf{R}), \quad (1)$$

with the momentum operators for the electronic (\mathbf{p}) and nuclear motion (\mathbf{P}), M being the proton mass. The potential energy is

$$\begin{aligned} V(\mathbf{r}, \mathbf{R}) = & \left(\frac{R}{R_c}\right)^4 + V^{en}(|\mathbf{r} - \mathbf{R}_1|) + V^{en}(|\mathbf{r} - \mathbf{R}_2|) \\ & + V^{en}(|\mathbf{r} - \mathbf{R}|) + V^{nn}(|\mathbf{R} - \mathbf{R}_1|) \\ & + V^{nn}(|\mathbf{R} - \mathbf{R}_2|) + V^{nn}(|\mathbf{R}_1 - \mathbf{R}_2|). \end{aligned} \quad (2)$$

Here, $\mathbf{R}_1 = (-L/2, 0)$ and $\mathbf{R}_2 = (L/2, 0)$ are the positions of the fixed ions, where we take $L = 4\sqrt{3}/5$ a.u., and the particle interactions are screened Coulomb-potentials of the form

$$V^{en}(\xi) = -\frac{1}{\sqrt{a + \xi^2}}, \quad V^{nn}(\xi) = \frac{1}{\sqrt{b + \xi^2}}, \quad (3)$$

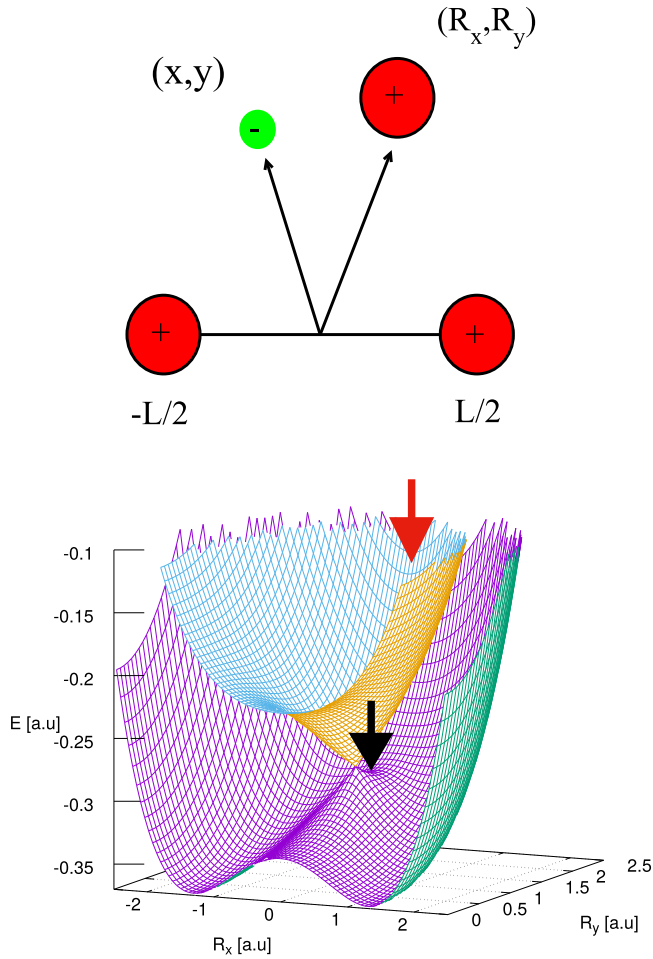


FIG. 1. Upper panel: The particle configuration of the model system: An electron (coordinates $\mathbf{r} = (x, y)$) and a proton (coordinates $\mathbf{R} = (R_x, R_y)$) move in a plane in the field of two additional but fixed protons at distances $\pm L/2$. Lower panel: Potential energy surfaces for two excited electronic states with quantum numbers $m = 1, 2$. The arrows mark the initial positions of the wave packets which lead to the density dynamics displayed in Figs. 4 and 6, respectively.

with $a = 0.5$ (a.u.)² and $b = 10.0$ (a.u.)². To ensure that the system remains bound, an extra quartic potential is added where the parameter $R_c = 3.5$ a.u. enters.

Born-Oppenheimer adiabatic potential energy surfaces $V_m(\mathbf{R})$ are defined as eigenvalues of the electronic Schrödinger equation,

$$\left[\frac{\mathbf{p}^2}{2} + V(\mathbf{r}, \mathbf{R}) \right] \varphi_m(\mathbf{r}; \mathbf{R}) = V_m(\mathbf{R}) \varphi_m(\mathbf{r}; \mathbf{R}), \quad (4)$$

with the electronic eigenfunctions $\varphi_m(\mathbf{r}; \mathbf{R})$. Using imaginary time-propagation,³¹ we calculate the potentials and the electronic wave functions for the first two excited states ($m = 1, 2$). The potentials are displayed in the lower part of Fig. 1. Clearly, the conical intersection at the D_{3h} symmetric configuration $\mathbf{R}_{CoIn} = (0, Y_{CoIn})$, with $Y_{CoIn} = \sqrt{3}L/2 (=1.2$ a.u.) can be seen.

To study the quantum mechanical motion, we solve the time-dependent Schrödinger equation,

$$i \frac{\partial}{\partial t} \psi(\mathbf{r}, \mathbf{R}, t) = H \psi(\mathbf{r}, \mathbf{R}, t), \quad (5)$$

imposing different initial conditions. This is done with the split-operator method³² on a four-dimensional grid. To achieve

convergent results, a grid ranging from -3 a.u. to 3 a.u. with $N^{(n)} = 101$ grid points is chosen for the nuclear degrees of freedom. For the electron coordinates, the grid covers the interval $[-12, +12]$ a.u., with $N^{(e)} = 81$ points.

The time-dependent wave function depends on four coordinates and to visualize its dynamics we examine the electronic ($\rho^{(e)}$) and nuclear ($\rho^{(n)}$) densities defined as

$$\rho^{(e)}(\mathbf{r}, t) = \int d\mathbf{R} |\psi(\mathbf{r}, \mathbf{R}, t)|^2, \quad (6)$$

$$\rho^{(n)}(\mathbf{R}, t) = \int d\mathbf{r} |\psi(\mathbf{r}, \mathbf{R}, t)|^2, \quad (7)$$

respectively. Expanding the wave function in terms of the adiabatic basis set defined by Eq. (4),

$$\psi(\mathbf{r}, \mathbf{R}, t) = \sum_{m'} \psi_{m'}(\mathbf{R}, t) \varphi_{m'}(\mathbf{r}; \mathbf{R}), \quad (8)$$

we obtain the adiabatic nuclear density in state (m) by projection

$$\rho_m^{(n)}(\mathbf{R}, t) = |\langle \varphi_m(\mathbf{r}; \mathbf{R}) | \psi(\mathbf{r}, \mathbf{R}, t) \rangle_{\mathbf{r}}|^2 = |\psi_m(\mathbf{R}, t)|^2. \quad (9)$$

The respective population then is

$$P_m(t) = \int d\mathbf{R} \rho_m^{(n)}(\mathbf{R}, t). \quad (10)$$

For the dynamics, we first set the initial condition

$$\psi(\mathbf{r}, \mathbf{R}, t = 0) = N e^{-\beta(R_x - R_{x,0})^2} e^{-\beta(R_{y,0} - R_0)^2} \varphi_2(\mathbf{r}; \mathbf{R}), \quad (11)$$

which represents a Gaussian wave packet in the nuclear degrees of freedom and we start in the $m = 2$ adiabatic state. Here, N is a normalization constant and the parameters are $\beta = 9$ (a.u.)⁻², $R_{x,0} = 0$, and $R_{y,0} = 2.1$ a.u. This choice localizes the initial wave packet in the middle between the two fixed ions ($R_{x,0} = 0$) with a displacement of $R_{y,0}$ along the $R_{y,0}$ -axis, which is above the conical intersection. The localization of the initial nuclear wave packet is indicated by a red arrow in Fig. 1, lower panel. The mean energy $\langle H \rangle = -0.1158$ a.u. is much higher than that of the CoIn at -0.2829 a.u.

In Fig. 2, upper panel, we show the populations in the two electronic states as a function of time (solid lines, case (a)). Starting in the second state, it is seen that after about two fs, a non-adiabatic transition takes place and population is transferred to the lower state ($m = 1$). The transfer proceeds ultrafast and it is completed within less than two fs. Regarding the densities displayed in Fig. 3, details of the dynamics are revealed. The left hand panels show the total nuclear density $\rho^{(n)}(\mathbf{R}, t)$ at selected times, as indicated. The initial Gaussian wave packet moves towards smaller values of R_y thereby remaining of almost constant shape. During the covered time interval, the conical intersection located at $\mathbf{R}_{CoIn} = (0, 1.2)$ a.u. is passed. This can clearly be seen in the state-specific nuclear densities $\rho_m^{(n)}(\mathbf{R}, t)$ which are shown in the middle and right hand panels of Fig. 3. Note, that the total density can be written as the sum of the two densities $\rho_m^{(n)}(\mathbf{R}, t)$. Between 2.3 and 3.2 fs, most of the density is transferred to the lower excited state which leaves a hole in the remaining density $\rho_2^{(n)}(\mathbf{R}, t)$. Figure 3 illustrates that, besides the dramatic changes which are present in the two nuclear density components (or the two nuclear components

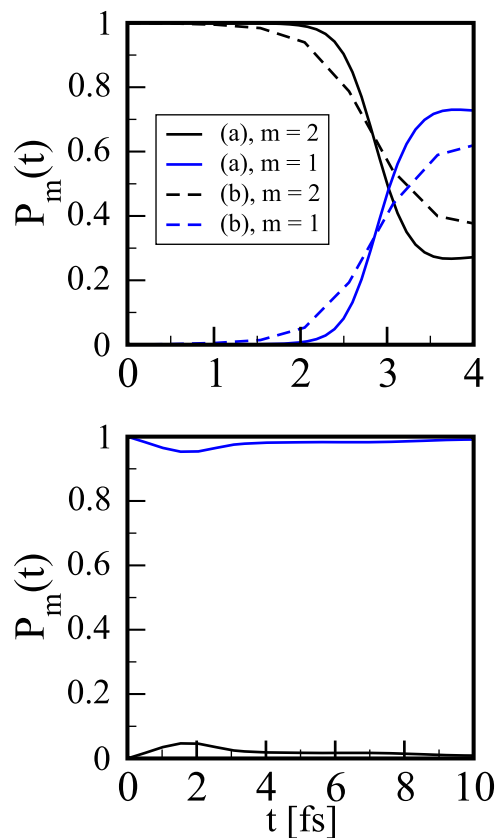


FIG. 2. Time-dependent populations $P_m(t)$ in the two adiabatic electronically excited states. The upper panel shows two cases where, starting in the upper state ($m = 2$), the CoIn is passed resulting in an efficient population transfer. In the situation (a), the nuclear wave packet is placed at $R_{x,0} = 0, R_{y,0} = 2.10$ a.u., and it is shifted to have its center at $R_{x,0} = 0.3$ a.u., $R_{y,0} = 1.72$ a.u. in the case (b). For an initial wave packet being prepared in the lower state ($m = 1$), only a small fraction of the population is temporarily transferred to the upper state (lower panel).

of the total wave function), the complete nuclear density is just a Gaussian moving along the R_y direction.

We now pose the question of what happens to the electron during the motion through the CoIn. Therefore, we compare, in Fig. 4, the nuclear density $\rho^{(n)}(\mathbf{R}, t)$ (left hand panels, same as in Fig. 3) with the electronic density $\rho^{(e)}(\mathbf{r}, t)$ (right hand panels). Also marked, as red circles, are the positions of the fixed ions and the position of the conical intersection (blue). To connect the time-evolution of the densities to the interaction potential, we include contours of averaged potentials defined as

$$\langle V^{(n)}(\mathbf{R}, t) \rangle = \int d\mathbf{r} V(\mathbf{R}, \mathbf{r}) \rho^{(e)}(\mathbf{r}, t), \quad (12)$$

$$\langle V^{(e)}(\mathbf{r}, t) \rangle = \int d\mathbf{R} V(\mathbf{R}, \mathbf{r}) \rho^{(n)}(\mathbf{R}, t). \quad (13)$$

The figure demonstrates that, as the proton moves, the averaged potential $\langle V^{(e)}(\mathbf{r}, t) \rangle$ does not change significantly in the region where the electronic density is non-zero. As a consequence, the latter remains almost constant and preserves its p_x -like orbital shape. This is not the case for the nuclear motion. There, the gradients of the potential $\langle V^{(n)}(\mathbf{R}, t) \rangle$ are such that the nuclear density is driven along the symmetry line $R_x = 0$, thereby showing only insignificant broadening. As a main result we find that

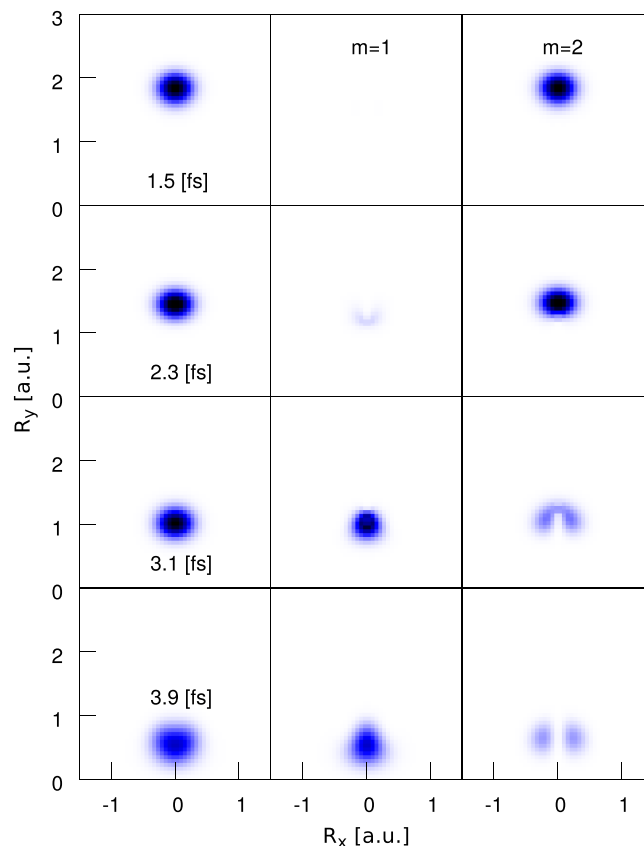


FIG. 3. Motion through the conical intersection. Shown are the total nuclear density $\rho^{(n)}(\mathbf{R}, t)$ (left hand panels) and the densities in the two adiabatic states $\rho_m^{(n)}(\mathbf{R}, t)$, as indicated.

the electron density is not influenced by the passage of the wave packet through the CoIn. This is the characteristic for a diabatic motion where electronic properties do not change as a function of the nuclear geometry. Note, however, that for a strictly diabatic dynamics, the population transfer should amount to 100%, whereas here, it is only about 70%. This accounts for the small temporal changes seen in the electron density. The fact that a nuclear wave packet passes essentially unchanged through a non-adiabatic region as a single Gaussian has the consequence that, in a mixed quantum/classical scheme, the population transfer/branching-ratio is correctly captured even when a single trajectory is used for the nuclear motion, as was found in Refs. 33 and 34.

The dynamics illustrated in Fig. 3 results from an initial nuclear wave packet being placed at $R_{x,0} = 0$. Then, this packet directly moves towards the CoIn along the $R_{y,0}$ direction and the nuclear density remains symmetric with respect to $R_x = 0$. To investigate what happens if this symmetry is broken, we place the initial wave packet at a position of $R_{x,0} = 0.30$ a.u., $R_{y,0} = 1.72$ a.u. As can be taken from Fig. 2, the population transfer (case (b)) is similar as in the above discussed case. The dynamics is illustrated in Fig. 5. It is seen that the nuclear density (left hand panels) now approaches the CoIn differently but, as in the former case, remains Gaussian-like during the time the passage takes place. The electronic density (right hand panels) is rotated at an angle of $\approx 20^\circ$ as compared to the symmetric situation and, as before, does not exhibit significant changes as the nucleus moves through the location of the CoIn.

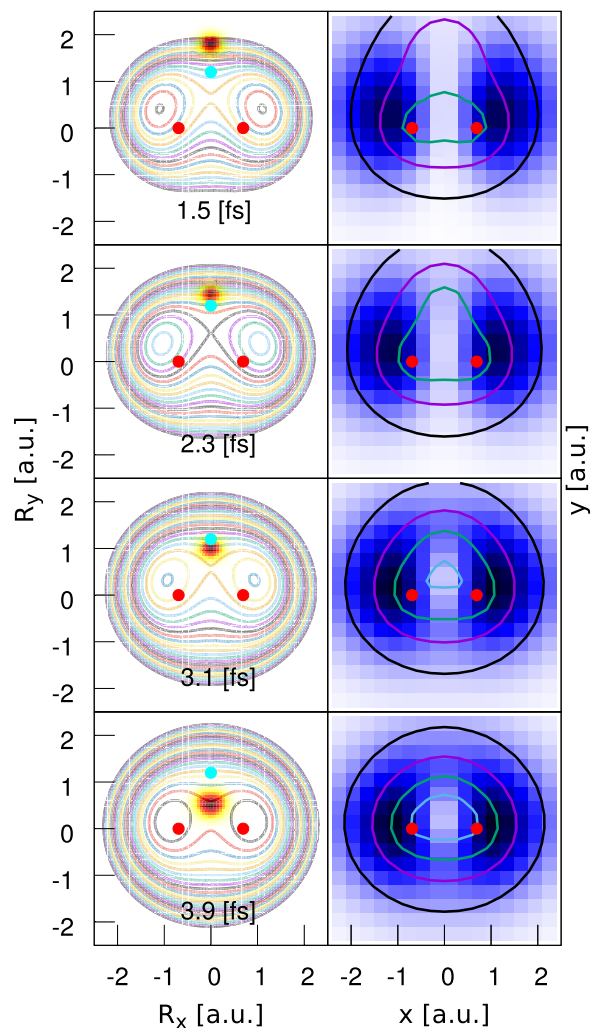


FIG. 4. Motion through the conical intersection. Shown are the total nuclear ($\rho^{(n)}(\mathbf{R}, t)$, left hand panels) and electronic density ($\rho^{(e)}(\mathbf{r}, t)$, right hand panels). The positions of the fixed nuclei and the conical intersection are marked by red and blue circles, respectively. The red circles in the right hand panels denote the positions where the electron is at the positions of the fixed nuclei. Also shown are contours of the averaged nuclear (left panels) and electronic (right panels) potentials defined in Eqs. (12) and (13). In the left hand panels, the contours start at an upper value of -0.7 a.u. and decrease in steps of 0.01 a.u. The lower values are -0.86 a.u. (1.5 fs), -0.89 a.u. (2.3 fs), -0.92 a.u. (3.1 fs), and -0.94 a.u. (3.9 fs), respectively. The contours in the right hand panels start at -0.5 eV (black line) and decrease in steps of 0.5 a.u.

For comparison, we also consider a case where the initial nuclear wave packet is the one defined in Eq. (11) but now we start in the lower excited state ($m = 1$) with wave function $\varphi_1(\mathbf{r}; \mathbf{R})$ and the displacement in R_y is $R_0 = 1.5$ a.u. (see Fig. 1, lower panel). For this choice, the mean energy $\langle H \rangle = -0.2835$ a.u. is slightly lower than the energy of the CoIn. This results in a dynamics being mainly restricted to the first excited state which means that the population $P_1(t)$ should be close to its initial value of one. The population dynamics shown in the lower panel of Fig. 2 indeed reveals that only a small fraction is temporarily transferred between the two adiabatic states. Figure 6 (left hand panels) documents that the nuclear density moves towards the CoIn and splits symmetrically into two parts. This motion is driven by the averaged potential $\langle V^{(n)}(\mathbf{R}, t) \rangle$ which, as a function of time, flattens substantially along the R_x -direction so that a large dispersion occurs. Because we here encounter the situation of a

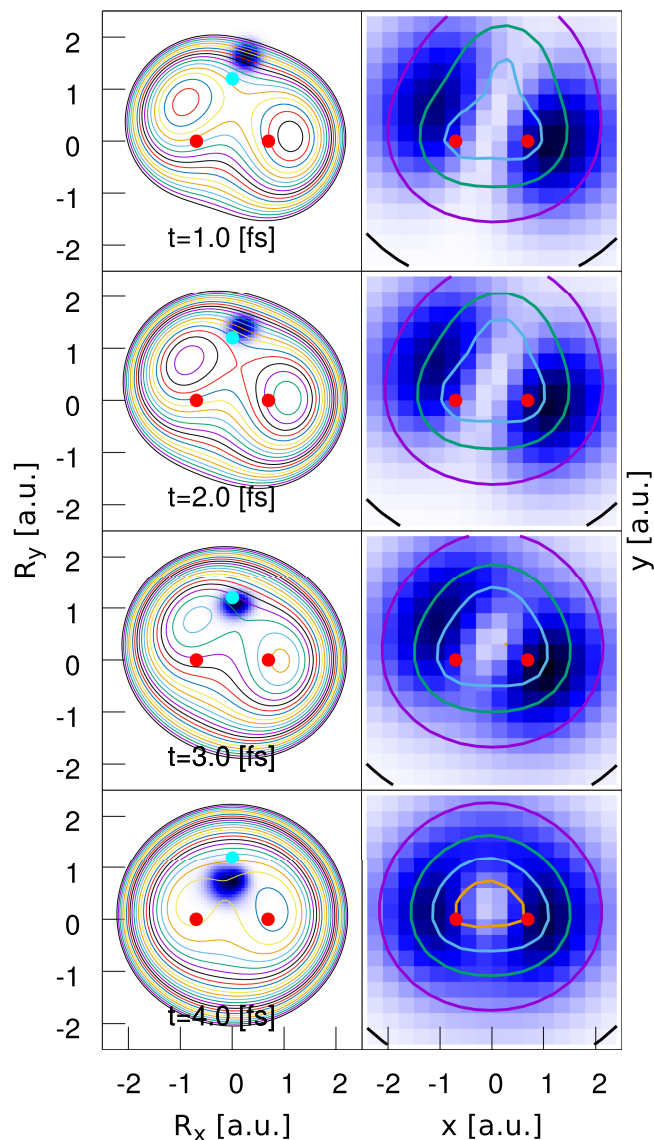


FIG. 5. Same as Fig. 4 but for an initial nuclear wave packet displayed from the symmetry line having its center at $R_{x,0} = 0.3$ a.u., $R_{y,0} = 1.72$ a.u.

motion in only a single adiabatic state, the nuclear motion may also be interpreted using the adiabatic potential $V_1(\mathbf{R})$. As can be taken from Fig. 1, the splitting is related to the barrier being present in this potential.

During the nuclear motion, the averaged potential $\langle V^{(e)}(\mathbf{r}, t) \rangle$ seen by the electron becomes steeper along the y -direction and flatter along the x -direction. The time-dependent gradients cause the electron density which initially is oriented along the y -axis, to localize along the x -axis. These changes proceed smoothly which indicates that the electron adiabatically adapts to the nuclear geometry. At a time of 10 fs, the two maxima of the nuclear density approximately correspond to the linear nuclear configuration. The moving proton is found with equal probability at positions of $\mathbf{R} \approx (\pm 1.8, 0)$ a.u., and the electronic density is mainly localized between these positions and those of the two fixed ions.

To conclude, we study the coupled electron-nuclear motion taking place in the vicinity of a conical intersection which is identified from the topology of two excited state potential energy surfaces. Starting in the higher adiabatic state,

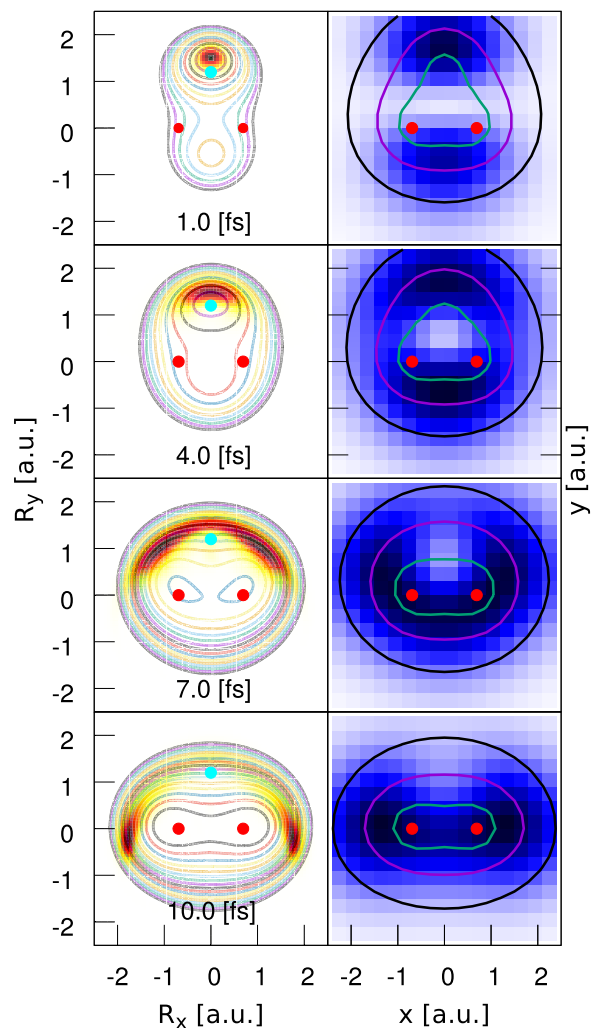


FIG. 6. Same as Fig. 4 but for the case of an adiabatic motion. The separation of the contours in the left hand panels is 0.01 a.u. and they start at an energy of -0.755 a.u. and end at -0.845 (1 fs, 4 fs), -0.905 a.u. (7 fs), and -0.915 a.u. (10 fs), respectively.

an ultrafast population transfer takes place upon passage of the wave packet through the configuration where the CoIn is located. Regarding the total nuclear and also the electronic density, no significant changes can be observed: the nuclear density reflects a localized wave-packet dynamics and the electronic density remains constant. On the contrary, defining the initial wave packet as having exclusively the character of the lower excited state results in an adiabatic motion where the electron density smoothly adapts to the nuclear position. In both cases, the fate of the time-dependent nuclear/electronic density can be related to potentials obtained by averaging the complete interaction potential over the electronic/nuclear density, respectively. To answer the question formulated at the beginning of the paper, the used model provides an example where the passage through a CoIn, if analyzed in terms of a wave packet motion in the complete electron-nuclear configuration space, does not show any reminiscence of this special topology. In particular, because the electron density does not change during the respective time-interval, one might conclude that the electron “does not care” about the conical intersection.

It has to be kept in mind that our conclusions are based on a one-electron model and a single moving nucleus both moving

in a plane. Besides the much more demanding numerical task which arises if more particles moving in three dimensions are to be described, for many-electron systems one has to include the exchange symmetry. This means that additional symmetry constraints have to be imposed on the initial electronic wave function. We do not believe that this changes much of the dynamical features illustrated in this paper because, as for the present system, they derive from the motion of a wave packet moving on a single potential energy surface. Nevertheless, we cannot prove this, and further research might be able to clarify this point.

Financial support by the DFG within the FOR 1809 is acknowledged.

- ¹A. Szabo and N. S. Ostlund, *Modern Quantum Chemistry* (McGraw-Hill, New York, 1989).
- ²T. Helgaker, P. Jørgensen, and J. Olsen, *Molecular Electronic Structure Theory* (Wiley, Chister, UK, 2000).
- ³M. Born and K. Huang, *Theory of Crystal Lattices* (Oxford University Press, London, 1954).
- ⁴R. Schinke, *Photodissociation Dynamics* (Cambridge University Press, Cambridge, 1993).
- ⁵D. J. Tannor, *Introduction to Quantum Mechanics: A Time-Dependent Perspective* (University Science Books, Sausalito, 2007).
- ⁶D. R. Yarkony, *Rev. Mod. Phys.* **68**, 985 (1996).
- ⁷*Conical Intersections: Electronic Structure, Dynamics and Spectroscopy*, edited by W. Domcke, D. R. Yarkony, and H. Köppel (World Scientific, Singapore, 2004).
- ⁸*Conical Intersections: Theory, Computation and Experiment*, edited by W. Domcke, D. R. Yarkony, and H. Köppel (World Scientific, Singapore, 2011).
- ⁹M. J. Paterson, M. J. Bearpark, M. A. Robb, L. Blancafort, and G. A. Worth, *Phys. Chem. Chem. Phys.* **7**, 2100 (2005).
- ¹⁰W. Domcke and D. R. Yarkony, *Adv. Chem. Phys.* **63**, 325 (2012).
- ¹¹B. G. Levine and T. Martinez, *Annu. Rev. Phys. Chem.* **58**, 613 (2007).
- ¹²W. Domcke and G. Stock, *Adv. Chem. Phys.* **100**, 1 (1997).
- ¹³D. A. Farrow, W. Qian, E. R. Smith, A. A. Ferro, and D. M. Jonas, *J. Chem. Phys.* **128**, 144510 (2008).
- ¹⁴D. Polli, P. Altoe, O. Weingart, K. M. Spillane, C. Manzoni, D. Brida, G. Tomasello, G. Orlandi, P. Kukura, R. A. Mathies *et al.*, *Nature* **467**, 440 (2010).
- ¹⁵T. J. Martinez, *Nature* **467**, 412 (2010).
- ¹⁶K. A. Kitney-Hayes, A. A. Ferro, V. Tiwari, and D. M. Jonas, *J. Chem. Phys.* **140**, 124312 (2014).
- ¹⁷J. Krčmar, M. F. Gelin, and W. Domcke, *J. Chem. Phys.* **143**, 074308 (2015).
- ¹⁸H. J. Wörner, J. B. Bertrand, B. Fabre, J. Higuier, H. Ruf, A. Dubrouil, S. Patchkovskii, M. Spanner, Y. Mairesse, V. Blanchet *et al.*, *Science* **334**, 208 (2011).
- ¹⁹M. Kowalewski, K. Bennett, K. E. Dorfman, and S. Mukamel, *Phys. Rev. Lett.* **115**, 193003 (2015).
- ²⁰W. Hua, S. Oesterling, J. Biggs, Y. Zhang, H. Ando, R. de Vivie-Riedle, B. P. Fingerhut, and S. Mukamel, *Struct. Dyn.* **3**, 023601 (2016).
- ²¹J. Albert, D. Kaiser, and V. Engel, *J. Chem. Phys.* **144**, 171103 (2016).
- ²²S. Shin and H. Metiu, *J. Chem. Phys.* **102**, 9285 (1995).
- ²³S. Shin and H. Metiu, *J. Phys. Chem.* **100**, 7867 (1996).
- ²⁴M. Erdmann, P. Marquetand, and V. Engel, *J. Chem. Phys.* **119**, 672 (2003).
- ²⁵M. Erdmann, E. K. U. Gross, and V. Engel, *J. Chem. Phys.* **121**, 9666 (2004).
- ²⁶M. Falge, V. Engel, and S. Gräfe, *J. Chem. Phys.* **134**, 184307 (2011).
- ²⁷M. Falge, V. Engel, and S. Gräfe, *J. Phys. Chem. Lett.* **3**, 2617 (2012).
- ²⁸A. Abedi, F. Agostini, Y. Suzuki, and E. K. U. Gross, *Phys. Rev. Lett.* **110**, 263001 (2013).
- ²⁹F. Agostini, A. Abedi, Y. Suzuki, S. Min, N. T. Maitra, and E. Gross, *J. Chem. Phys.* **142**, 084303 (2015).
- ³⁰S. K. Min, A. Abedi, K. Kim, and E. K. U. Gross, *Phys. Rev. Lett.* **113**, 263004 (2014).
- ³¹R. Kosloff and H. Tal-Ezer, *Chem. Phys. Lett.* **127**, 223 (1986).
- ³²M. D. Feit, J. A. Fleck, and A. Steiger, *J. Comput. Phys.* **47**, 412 (1982).
- ³³F. Agostini, A. Abedi, and E. K. U. Gross, *J. Chem. Phys.* **141**, 214101 (2014).
- ³⁴A. Abedi, F. Agostini, and E. K. U. Gross, *Europhys. Lett.* **106**, 33001 (2014).